BIOCHEMISTRY
including biophysical chemistry & molecular biology

 Volume 48, Number 15 April 21, 2009

Structural and Chemical Basis for Glucosamine 6-Phosphate Binding and Activation of the *glmS* Ribozyme[†,‡]

Jesse C. Cochrane,[§,||] Sarah V. Lipchock,[⊥] Kathryn D. Smith,[⊥] and Scott A. Strobel*[,§,⊥]

Departments of Molecular Biophysics and Biochemistry and Chemistry, Yale University, New Haven, Connecticut 06520

Received November 7, 2008; Revised Manuscript Received February 13, 2009

ABSTRACT: The *glmS* ribozyme is the first naturally occurring catalytic RNA that relies on an exogenous, nonnucleotide cofactor for reactivity. From a biochemical perspective, the *glmS* ribozyme derived from *Bacillus anthracis* is the best characterized. However, much of the structural work to date has been done on a variant *glmS* ribozyme, derived from *Thermoanaerobacter tengcongensis*. Here we present structures of the *B. anthracis glmS* ribozyme in states before the activating sugar, glucosamine 6-phosphate (GlcN6P), has bound and after the reaction has occurred. These structures show an active site preorganized to bind GlcN6P that retains some affinity for the sugar even after cleavage of the RNA backbone. A structure of an inactive *glmS* ribozyme with a mutation distal from the ligand-binding pocket highlights a nucleotide critical to the reaction that does not affect GlcN6P binding. Structures of the *glmS* ribozyme bound to a naturally occurring inhibitor, glucose 6-phosphate (Glc6P), and a nonnatural activating sugar, mannosamine 6-phosphate (MaN6P), reveal a binding mode similar to that of GlcN6P. Kinetic analyses show a pH dependence of ligand binding that is consistent with titration of the cofactor's phosphate group and support a model in which the major determinant of activity is the sugar amine independent of its stereochemical presentation.

The *glmS* ribozyme catalyzes a reaction that is chemically identical to that of other nucleolytic ribozymes but uses a novel catalytic strategy (Figure 1A) (*1*). In the nucleolytic cleavage reaction the 2′-OH of a ribose acts as the nucleophile, attacking the scissile phosphate and releasing the 5′-oxygen leaving group (Figure 1B). This reaction requires an in-line (180°) conformation for the 2′-OH, scissile phosphate, and 5′-oxygen. The reaction is often accelerated through activation of the nucleophile, stabilization of the transition state, or protonation of the leaving group (*1*). Many nucleolytic ribozymes use nucleobases and metal ions to fulfill these roles (*2*). In the *glmS* ribozyme, a guanosine has been implicated in the reaction mechanism (Figure 1B) (*3, 4*). However, the *glmS* ribozyme is the first identified example of a nucleolytic RNA that also relies on a small molecule cofactor, glucosamine 6-phosphate (GlcN6P),[1] to promote chemistry (Figure 1C) (*5*). The *glmS* ribozyme is found upstream of the gene for glucosamine 6-phosphate synthase, the enzyme responsible for GlcN6P production (*5*). This RNA is also a riboswitch, regulating the cellular production of GlcN6P.

Riboswitches are a recently identified class of RNAs that function as regulators of gene expression (*6*). In most cases, the riboswitch is located in the 5′-untranslated region (UTR)

[†] This work was supported by a grant from the National Science Foundation (MCB0544255) to S.A.S.

[‡] Atomic coordinates and structure factors have been deposited in the Protein Data Bank, www.rcsb.org, under accession codes 3G8S, 3G9C, 3G8T, 3G95, and 3G96.

* To whom correspondence should be addressed. Phone: (203) 432-9772. Fax: (203) 432-5767. E-mail: scott.strobel@yale.edu.

[§] Department of Molecular Biophysics and Biochemistry, Yale University.

[||] Present address: Department of Molecular Biology, Massachusetts General Hospital, and Department of Genetics, Harvard Medical School, Boston, MA 02114.

[⊥] Department of Chemistry, Yale University.

[1] Abbreviations: *B. anthracis*, *Bacillus anthracis*; GlcN6P, glucosamine 6-phosphate; Glc6P, glucose 6-phosphate; MaN6P, mannosamine 6-phosphate; *T. tengcongensis*, *Thermoanerobacter tengcongensis*; *UTR, untranslated region; TLC, thin-layer chromotography*.

10.1021/bi802069p CCC: $40.75
Published on Web 02/19/2009

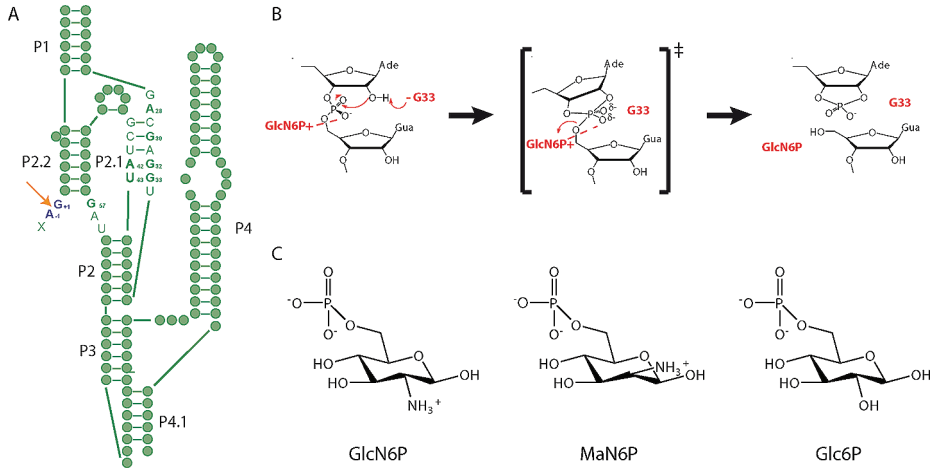

FIGURE 1: Structure and mechanism of the *glmS* ribozyme. (A) Secondary structure of the precleaved *glmS* ribozyme. Green filled circles represent individual nucleotides, and key active site nucleotides are indicated. The cleavage site is shown using an orange arrow, and the nucleotides flanking the scissile phosphate are shown in dark blue. Paired regions are numbered according to convention. (B) The proposed catalytic mechanism of the *glmS* ribozyme. (C) The three sugars used in the mechanistic and structural studies.

of a gene that is involved in regulating the concentration of the small molecule that the riboswitch binds (*7*). Upon ligand binding, a conformational change occurs that is propagated along the mRNA leading to decreased (or increased) gene production using a variety of mechanisms, including the formation of a transcriptional terminator or seclusion of the Shine−Dalgarno sequence (*7*). However, even the earliest reports of the *glmS* ribozyme suggested that as a riboswitch it was using a different mechanism (*5*). First, addition of GlcN6P induced a specific cleavage event in the 5′-UTR of the *glmS* gene, which seemed to be correlated with gene expression levels. Second, there did not appear to be any structural rearrangements in the RNA upon addition of GlcN6P (*5, 8*).

Initial crystallographic studies of the *glmS* ribozyme added evidence to support a different mode of action for this riboswitch (*3, 9*). The structure of a precleaved version of the *glmS* ribozyme from *Thermoanaerobacter tengcongensis* was very similar to the structure of the ribozyme bound to the competitive inhibitor, glucose 6-phosphate (Glc6P) (*9*). Glc6P is structurally identical to GlcN6P but has a hydroxyl at C2 instead of a primary amine (Figure 1C). Furthermore, all precleaved, postcleavage, and effector bound structures solved to date show very similar active sites, supporting the biochemical conclusion that there is little difference between the unbound, bound, and reacted forms of the ribozyme (*3, 5, 8*−*10*).

However, despite the similar active sites, there are some differences in the peripheral regions of the ribozyme between the *T. tengcongensis* structures and the effector bound *Bacillus anthracis* structure (*3, 10*). These may have arisen because the ribozymes were derived from different sources or because different substitutions were made to inhibit the ribozyme. Because the majority of the biochemical characterization of the *glmS* ribozyme has been done using the *B. anthracis* sequence, it is important to examine the structure of this form of the ribozyme throughout the catalytic cycle and with inactivating mutations.

The *glmS* ribozyme appears to be poised for catalysis, even in the absence of ligand binding, raising the question of how effector selectivity is achieved by the ribozyme (*9*). Klein et al. demonstrated the importance of a guanosine at the nucleotide 3′ of the scissile phosphate, showing that mutation of that nucleotide led to reduced affinity for GlcN6P over other ligands with primary amines (*10*). Here we present the crystal structures of a series of *glmS* ribozymes, providing snapshots of the full catalytic pathway for the *B. anthracis* variant of the riboswitch as well as highlighting important aspects of GlcN6P binding. Additional biochemical data explore the fine control the ribozyme exerts in recognition of the sugar ligand for catalysis.

MATERIALS AND METHODS

Materials. RNA expression constructs were developed, synthesized, and purified as previously described (*3*). Glucosamine 6-phosphate (GlcN6P) and glucose 6-phosphate (Glc6P) were purchased from Sigma-Aldrich (St. Louis, MO). Mannosamine 6-phosphate (MaN6P) was synthesized enzymatically, using a modified procedure based on that of Liu and Lee (*11*). Briefly, 2 mmol (0.43 g) of 2-amino-2-deoxy-D-mannose hydrochloride was combined with 1.4 mmol (0.29 g) of $MgCl_2 \cdot 6H_2O$ and 2.2 mmol (1.21 g) of ATP in 54 mL of deionized water. Hexokinase (1320 units, 13 mg) from *Saccharomyces cerevisiae* was dissolved in 1 mL of deionized water and added to this mixture. The reaction was stirred for 5 h at room temperature, and the pH was kept constant at 7.5. The product appeared as a UV-negative, ninhydrin-positive spot with a lower R_f value than the starting material when visualized by thin-layer chromatography (TLC). When complete, the reaction mixture was lyophilized and then resuspended in a minimal amount of water (approximately 5 mL) and the pH adjusted to 5. Purification was performed using a Dowex 50W X8 column (200−400 mesh, H^+ form) washed one time with water and two times with 1 M HCl and then equilibrated with water until it reached pH 5. The compound was eluted with water, and purity was verified by TLC analysis. MaN6P was checked for nuclease contamination prior to use.

Methods. Crystallization. Complexes were prepared for crystallization, with the exception of the MaN6P containing crystals, following the previously published method (*3*). MaN6P crystals were grown at higher pH, using TAPS (pH 8.5) instead of sodium cacodylate (pH 6.8) and 5−20 mM

MaN6P. Crystals were harvested and frozen in 35% PEG-8000, 1.5 M 1,6-hexanediol, 200 mM KCl, 20 mM $MgCl_2$, and 20 mM TAPS (pH 8.5). The freezing solution had to be readjusted to pH 8.5 after all components were added. All data collection was done at Brookhaven National Laboratory. Data were processed using HKL-2000, and molecular replacement was done using PHASER (*12, 13*). REFMAC and COOT were used for the rebuilding and refinement of all crystallographic data (*14*−*16*). All structural figures were made using PYMOL (*17*).

Kinetics. Ban-11U RNA (*B. anthracis glmS* ribozyme construct) (1 μM) was incubated with 5′ end radiolabeled rS (substrate oligonucleotide containing a ribose at the cleavage site) in kinetics buffer (100 mM $MgCl_2$, 25 mM potassium acetate, 25 mM potassium cacodylate, 25 mM K-HEPES, 25 mM TAPSO, adjusted to the appropriate pH) for ~5 min. GlcN6P or MaN6P, pH adjusted, was added to start the reaction. Aliquots were taken at appropriate times, either by hand or using a quench flow apparatus (KinTek Corp., Austin, TX), and quenched using formamide loading buffer (95% formamide, 2.5 mM EDTA, 0.1% bromophenol blue, 0.1% xylene cyanol) or formamide loading buffer with 100 mM EDTA for the quench flow experiments. Reactant and product rS were separated by denaturing polyacrylamide gel electrophoresis and visualized using a STORM PhosphorImager (GE Healthcare, Piscataway, NJ). Data were analyzed using ImageQuant (GE Healthcare, Piscataway, NJ), and rates were determined using the equation:

$$f = (1 - f_\infty)\exp(-k_{obs}t) + f_\infty \quad (1)$$

where f = fraction unreacted, f_∞ = fraction unreacted at $t = \infty$, and t = time and fit using the least-squares implementation in KaleidaGraph (Synergy Software, Reading, PA). $K_{1/2}$ (concentration of sugar required to achieve half-maximal rate) and k_{max} (maximum rate of cleavage) at each pH were determined using the equation:

$$k_{obs} = (k_{max}C)/(C + K_{1/2}) \quad (2)$$

where C = concentration of sugar. The apparent pK_a's for $1/K_{1/2}$, k_{max}, and $k_{max}/K_{1/2}$ were determined using the equation:

$$y = \frac{y_{max}K_a^{\,m}}{[H^+]^m + K_a^{\,m}} \quad (3)$$

where y is $1/K_{1/2}$, k_{max}, or $k_{max}/K_{1/2}$ and y_{max} is the maximum value for $1/K_{1/2}$, k_{max}, or $k_{max}/K_{1/2}$ over the entire pH range. In all cases the slope, m, was set to 1 except in the case of k_{max} for *glmS* cleavage catalyzed by GlcN6P.

Three independent kinetic trials were run for each sugar concentration at every pH, and K_a's were determined from the average of the trials, represented in Figure 6. Reported error is the calculated standard error from the three trials and displayed as error bars in Figure 6.

^{31}P NMR Titration. NMR samples containing GlcN6P were titrated using KOH and brought to a final concentration of 50 mM cofactor and 50% D_2O, in the absence of the ribozyme. A total of 11 samples were used between pH 4.2 and pH 8.4. A 1D ^{31}P spectrum with composite-pulse proton decoupling was collected on a 500 MHz Bruker Advance NMR spectrometer running TopSpin version 1. The pH was measured before and after the NMR experiment, and the two measured values were averaged to give a pH for each sample; however, only the pH of the samples initially at pH 4.2 and 8.4 changed over the course of the experiment. The K_a of the phosphate group was calculated using the equation:

$$\Delta\omega = \frac{\Delta\omega_{max}K_a}{[H^+] + K_a} \quad (4)$$

where $\Delta\omega$ is the change in ^{31}P chemical shift.

RESULTS

All structures reported here were derived from crystals that grew in conditions similar to the original published condition for the *B. anthracis glmS* ribozyme (*3*). The data collection and refinement statistics are summarized in Supporting Information Table S1. For a list of all *glmS* ribozyme structures determined to date, see Supporting Information Table S2. All ribozyme crystallization complexes were composed of an RNA transcript, an oligonucleotide with a 2′-*O*-methyladenosine at the cleavage site, and the RNA binding domain of the U1A protein, unless otherwise noted. All crystals were in the $P2_1$ space group with four molecules in the asymmetric unit. In most cases, the overall architecture of the active sites of the four molecules was the same. Any differences observed between the four are mentioned explicitly in the discussion of each structure.

Structure of the Precleaved glmS. The structure of a *glmS* ribozyme derived from *B. anthracis* in the absence of cofactor was solved and refined to 3.1 Å resolution. The overall structure is similar to that of our previously reported structure of the ribozyme bound to the natural ligand, GlcN6P (Figure 2A,B) (*3*). The average rms deviation between the two structures is less than 1.5 Å. This apo-*glmS* structure, like a structure of the apo-*glmS* ribozyme derived from *T. tengcongensis*, reveals an active site architecture that is poised for catalysis (*9*). Even in the absence of sugar binding, all atoms involved in bond making and bond breaking are aligned for chemistry. The 2′-OH (methylated in this construct to inhibit the reaction), the scissile phosphate, and the 5′-O leaving group are at an angle of approximately 155°, very close to the in-line conformation required for nucleolytic attack (Figure 2A).

The sugar-binding pocket is structurally similar to that which was observed in the GlcN6P bound state of the ribozyme (*3*). P2.1 and P2.2, where most of the nucleotides that interact with GlcN6P are located, are superimposable in the presence or absence of sugar (Figure 2A,B). Further, the conserved guanosine (G33) that has been predicted to activate the nucleophile is still within hydrogen-bonding distance of the methylated 2′-OH (*3, 9*).

Structure of the Product glmS Complex. The crystal structure (2.9 Å resolution) of the product state of the *glmS* ribozyme was obtained from crystals containing the RNA transcript, U1A, GlcN6P, and an all ribose substrate oligonucleotide (rS). The substrate was fully cleaved during the precrystallization incubation time, and only the product was observed in the crystals (Figure 2C).

In this structure of the *B. anthracis* product ribozyme the GlcN6P appears to be bound in at least one of the four active

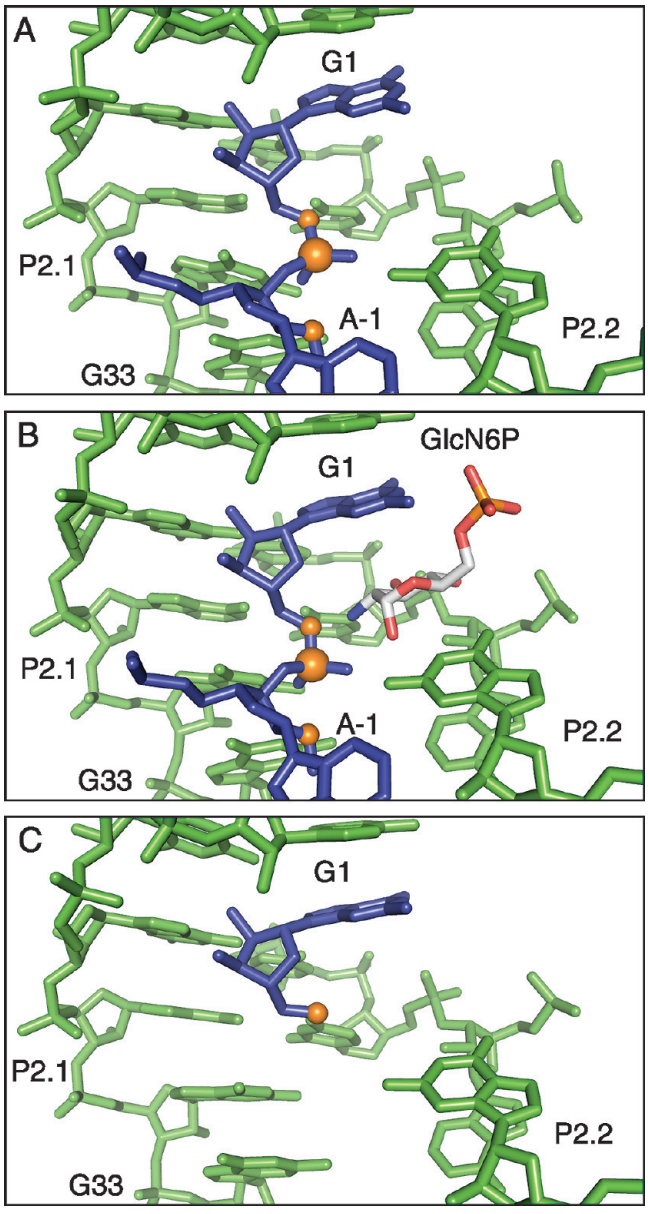

FIGURE 2: Active site of the *glmS* ribozyme through the cleavage reaction. (A) The active site structure of the unbound, precleaved state of the *glmS* ribozyme. The ribozyme is depicted in green, with the nucleotides that flank the scissile phosphate in blue and the reactive atoms shown in orange. This coloring scheme is used throughout the figures. (B) The active site structure of the GlcN6P bound state of the *glmS* ribozyme. The bound sugar molecule is depicted in gray. (C) The active site of the reacted state of the *glmS* ribozyme.

sites present within the asymmetric unit (Figure 3A); there is clear density for the phosphate and entire sugar which is positioned as it is in the precleaved structure (Figure 3B,C). The C2 primary amine, which has been implicated in the catalytic mechanism, is positioned between the free 5′-OH and the O4 of U43 (Figure 3B) (*5, 18*). There is also weak density for what appears to be the phosphate atom in the other three active sites, but it was modeled as a water molecule due to a lack of density for the sugar ring.

Structure of an Inactive Mutant glmS Ribozyme. The initial structures of the *glmS* ribozyme implicated a conserved guanosine, G33 (G40 in *T. tengcongensis*), in activation of the nucleophile (*3, 9*). Mutation of the G to any other nucleotide severely decreases the rate of the reaction (*3, 4*). The G to A mutant is the most detrimental and reduces the rate of the reaction by about 10^5. While this nucleotide has been implicated in catalysis, we cannot rule out the possibility that the effect may be due to a gross structural rearrangement in the active site. To address this question, we determined the structure of the mutant ribozyme in which this nucleotide was mutated to an adenosine (G33A).

The overall structure of a precleaved, G33A mutant (3.0 Å) has an average rmsd less than 2 Å from the structure of the wild-type ribozyme (Figure 4). Even the position of nucleotide 33 is essentially superimposable between the two structures. There is less than a 1 Å shift between the N1 of A33 and the N1 of G33; this shift moves A33 to a position that is slightly out of hydrogen-bonding distance to the methylated 2′-OH nucleophile (Figure 4). However, it does not disrupt the inline conformation of the nucleophile, scissile phosphate, and leaving group or affect GlcN6P binding to the ribozyme as there is clear density for the sugar molecule in every active site.

Structure of the glmS Ribozyme Bound to a Competitive Inhibitor. Previous structural and biochemical work has shown that the *glmS* ribozyme binds to, but is not activated by, a GlcN6P analogue, glucose 6-phosphate (Glc6P), in which the primary amine is replaced by a hydroxyl (*5, 9, 18*). We determined the structure of the precleaved form of the *B. anthracis* ribozyme bound to the Glc6P inhibitor (2.85 Å). As in the structure of the *T. tengcongensis glmS* ribozyme, there is strong density for Glc6P in the sugar-binding pocket of the *B. anthracis* structure (*9*). Glc6P occupies an almost identical position in the *glmS* ribozyme active site as GlcN6P, with perhaps a small shift (less than 1 Å) of the sugar away from the scissile phosphate (*3*). This sugar variant makes a set of contacts with the ribozyme similar to that made by the cognate ligand including a hydrogen bond between the O4 of U43 and the C2-hydroxyl of Glc6P (Figure 5A).

Structure of the glmS Ribozyme Bound to a Nonnatural, Activating Sugar. Breaker and co-workers reported that the *glmS* ribozyme could also be activated by mannosamine 6-phosphate (MaN6P), a GlcN6P analogue in which the stereochemistry at the C2-amine is inverted (*19*). We have determined the structure of MaN6P bound to the *B. anthracis glmS* ribozyme at 3.0 Å resolution. Due to limitations of sugar solubility in the freezing conditions, 5 mM MaN6P was used in the study. This concentration is below the measured $K_{1/2}$ for MaN6P (see below); however, density was observed for this sugar in at least two of the four *glmS* ribozymes present in the asymmetric unit. While the stereochemistry at C2 is inverted, the overall position of the sugar in the active site is similar to that of GlcN6P (Figure 5B). In fact, the C2-amine is still within hydrogen-bonding distance of the 5′-oxygen leaving group, fulfilling the proposed role of the primary amine in protonation of the leaving group.

Kinetic Analysis of GlcN6P Activation of the glmS Ribozyme. In our initial report of the *B. anthracis* ribozyme structure, we measured kinetic constants for activation of the ribozyme by GlcN6P (*3*). We found that the order of addition (i.e., whether the reaction begins by addition of labeled oligonucleotide or by addition of GlcN6P) impacts the rate of the reaction. The k_{max} plateaus at a slower rate when the reaction is initiated with labeled oligonucleotide

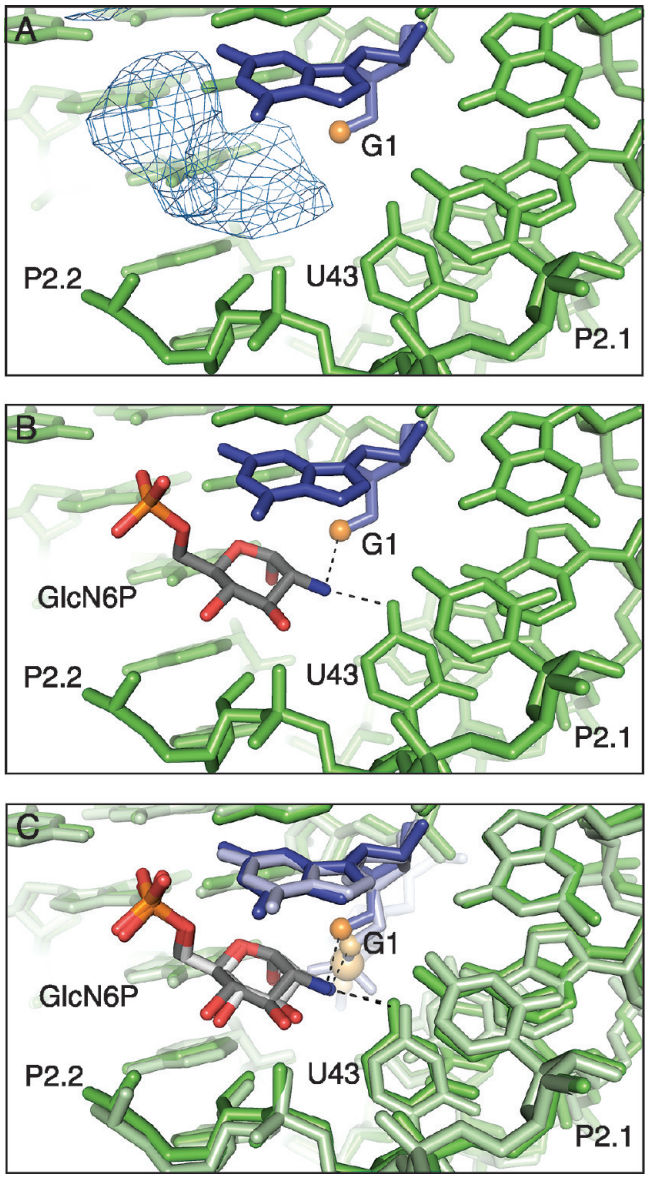

FIGURE 3: The active site of the product state of the *glmS* ribozyme. (A) $F_o - F_c$ density in the active site of the cleaved *glmS* ribozyme contoured at 2σ. (B) GlcN6P modeled into the active site of the cleaved *glmS* ribozyme. (C) The active site of the cleaved *glmS* ribozyme superimposed on the active site of the precleaved *glmS* ribozyme. The precleaved ribozyme is shown in lighter shades.

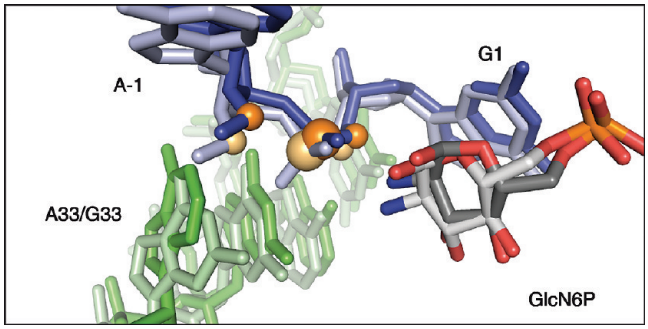

FIGURE 4: The active site of the G33A mutant *glmS* ribozyme superimposed on the active site of the wild-type *glmS* ribozyme. The mutant is shown in dark shades, and wild-type ribozyme is shown in light shades.

than when the reaction is initiated with GlcN6P. We attributed this to slow binding of the oligonucleotide or a conformational change that dominated the rate of the reaction under saturating conditions of GlcN6P. The complex is formed in ~1 min (data not shown); therefore, a preincubation time of ~5 min was used to ensure complete complex formation. We also revisited other aspects of the reaction conditions. First, we observed that under the conditions used, increasing the concentration of the ribozyme 10-fold did not affect the rate of the reaction, suggesting that the ribozyme concentration is saturating for the oligonucleotide substrate. Second, we were concerned about the free magnesium concentration in the reaction, particularly at high concentrations of sugar analogues. Initial reactions were carried out in 10 mM $MgCl_2$; however, we noticed that the reaction rate plateaus and then decreases when the concentration of $MgCl_2$ is less than or equal to the concentration of sugar phosphate (data not shown). This was attributed to free GlcN6P coordinating Mg^{2+} in solution and inhibiting the reaction. To ensure that Mg^{2+} did not become limiting at any of the reaction conditions, 100 mM $MgCl_2$ was used in all kinetic reactions. This change resulted in less than a 2-fold rate change at low concentrations of GlcN6P (data not shown).

We examined the reaction kinetics, initiating the reaction with GlcN6P and measuring the rate under conditions where the proposed conformational change is no longer rate limiting. Both k_{max} (the maximum rate of cleavage) and $K_{1/2}$ (concentration of sugar required to achieve half-maximal rate) showed a dependence on pH, with tighter binding and a faster rate at high pH (Figure 6A,B). At high pH, k_{max} plateaus at ~5 s^{-1}. The data do not fit to a curve with a slope fixed at 1 but fit nicely to a curve with a slope of 0.7 (Figure 6A). This indicates that the kinetics are more complex than can be described by a simple system with a single pK_a. A plot of $k_{max}/K_{1/2}$, however, fits very well to the titration of a group with pK_a ~7.5 (Figure 6C). These data suggest that the amine of GlcN6P (pK_a ~8) could be playing a key role as either an acid or a base in the ribozyme reaction. The $K_{1/2}$ data indicate that cofactor binding is relatively weak, with a $K_{1/2}$ of 1−2 mM from pH 7 to pH 9 (Supporting Information Figure S1). Binding of GlcN6P is even weaker at low pH, with a $K_{1/2}$ of ~6 mM at pH 5.5 (data not shown). A plot of $1/K_{1/2}$ versus pH reveals a pK_a of ~6.3. There are no groups within the RNA that have a pK_a near 6, but the pK_a of the phosphate of GlcN6P is expected to be in this range. The pK_a of GlcN6P was determined by collecting the phosphorus NMR spectrum of free GlcN6P at a variety of pHs. This revealed a pK_a for unbound GlcN6P of ~6.1 (Supporting Information Figure S2). The correlation between the pK_a of the phosphate of GlcN6P and the pK_a of GlcN6P binding to the *glmS* ribozyme suggests that titration of this phosphate may inhibit binding of GlcN6P to the *glmS* ribozyme.

Kinetic Analysis of MaN6P Activation of the glmS Ribozyme. We examined the ability of MaN6P to activate the *glmS* ribozyme under single turnover conditions. We measured the k_{max} for the reaction and found that it increases with increasing pH, plateaus at about 0.7 s^{-1}, and has an apparent pK_a of ~7.8 (Figure 6D). This rate is only about 7-fold slower than for activation by GlcN6P and has a pK_a in the same range. However, the $K_{1/2}$ for MaN6P for the *glmS* ribozyme is higher than that for GlcN6P. The highest concentration of MaN6P used in this analysis was 50 mM, which limits the accuracy with which we are able to

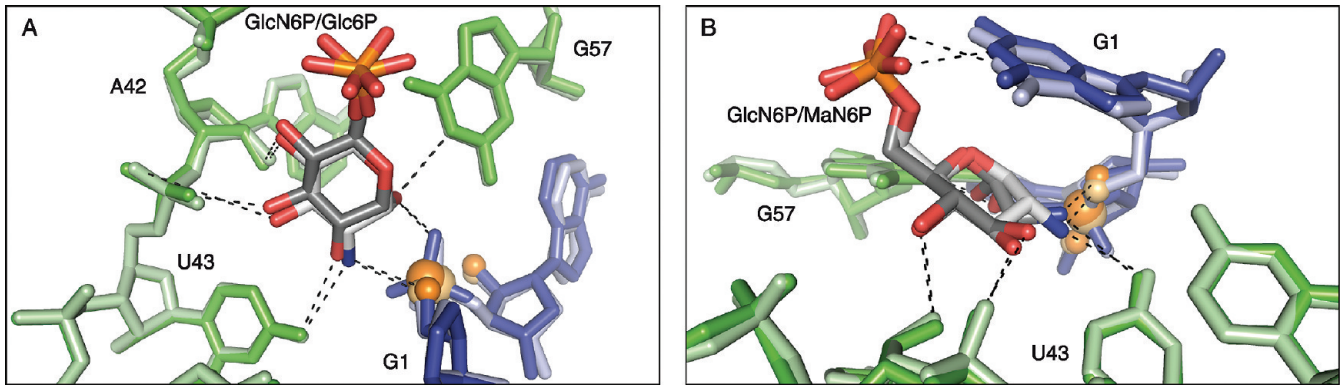

FIGURE 5: Alternative sugar binding in the active site of the *glmS* ribozyme. (A) The Glc6P bound active site of the *glmS* ribozyme superimposed on the GlcN6P bound active site. The Glc6P bound structure is shown in dark shades, and the GlcN6P bound structure is shown in light shades. (B) The MaN6P bound active site of the *glmS* ribozyme superimposed on the GlcN6P bound active site. The MaN6P bound structure is shown in dark shades, and the GlcN6P bound structure is shown in light shades.

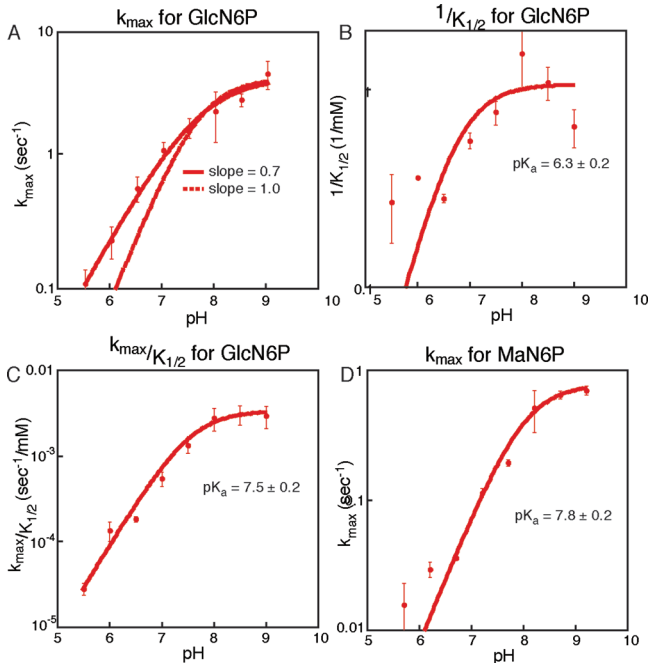

FIGURE 6: Kinetic analysis of GlcN6P and MaN6P activation of the *glmS* ribozyme. (A) Plot of pH versus average k_{max} for GlcN6P activation of the *glmS* ribozyme. Three independent kinetic trials were run for each concentration at each pH, and three independent values of k_{max} were determined; the average of the three values is depicted. Error bars represent the standard error on the average. In solid red is the best fit to the data, producing a slope of 0.7. The dotted line is the fit to the same data but forcing the slope of the line to be 1. (B) Plot of pH versus $1/K_{1/2}$ for GlcN6P activation of the *glmS* ribozyme. Three independent kinetic trials were run for each concentration at each pH, and three independent values of $1/K_{1/2}$ were determined; the average of the three values is depicted. Error bars represent the standard error on the average. Three independent pK_a's were calculated, and the average value is given; reported error is the standard error on the average. (C) Plot of pH versus $k_{max}/K_{1/2}$ for GlcN6P activation of the *glmS* ribozyme. As in plot B the values given are averages, and errors and error bars represent the standard error of three trials. (D) Plot of pH versus k_{max} for MaN6P activation of the *glmS* ribozyme. As in plot B the values given are averages, and errors and error bars represent the standard error of three trials.

determine the $K_{1/2}$. In fact, at all pHs the $K_{1/2}$ was too large to be measured accurately, but it is at least 15 mM and is possibly higher than 50 mM (Supporting Information Figure S3).

DISCUSSION

The *glmS* ribozyme binds GlcN6P leading to self-scission of the RNA backbone. However, unlike other riboswitch ligands that induce a conformational change in the RNA upon binding, the role of GlcN6P appears to be entirely chemical (*5, 8*). We have solved a series of crystal structures of the *glmS* ribozyme that show that the active site is preorganized in the absence of GlcN6P. In fact, we observe some residual binding of GlcN6P to the product state of the ribozyme, suggesting that many of the ribozyme elements required for GlcN6P binding are retained following cleavage (Figure 3). Additionally, mutation of a key guanosine predicted to activate the nucleophile of the reaction does not affect GlcN6P binding or significantly alter the conformation of the active site (Figure 4). New kinetic analysis further supports this conclusion, as the pK_a of $k_{max}/K_{1/2}$ for the reaction is consistent with the amine of GlcN6P playing a key role in catalysis (Figure 6). Structures of the *glmS* ribozyme bound to sugar variants of GlcN6P, including the activating sugar, MaN6P, and the nonactivating sugar, Glc6P, suggest that the ribozyme uses both catalytic and structural mechanisms to select against incorrect ligands (Figure 5). Additionally, we measured the rate of *glmS* ribozyme activity in the presence of MaN6P, a diastereomer of GlcN6P with inverted stereochemistry at the amine (Figure 6). This kinetic analysis demonstrates that the *glmS* ribozyme binds and is activated by MaN6P but at higher concentrations than GlcN6P, consistent with the structure of the *glmS* ribozyme bound to MaN6P (Supporting Information Figures S1 and S3).

GlcN6P Recognition through the Catalytic Cycle of the glmS Ribozyme. Previous biochemical and structural work indicated that the active site of the *glmS* ribozyme is almost fully formed even in the absence of bound ligand (*5, 8, 9*). Unlike other riboswitches, no large structural rearrangements upon binding could be detected using any solution technique (*5, 8*). This deviation from the traditional mode of ligand binding by riboswitches may also contribute to the low affinity binding of GlcN6P by the *glmS* ribozyme (Figure 6). Other riboswitches tend to have high affinity for their cognate ligands, with K_d's as low as 1 nM (*20*). Even the glycine riboswitch, which has one of the weakest reported affinities, binds glycine

with a K_d of around 30 μM (*20, 21*). In contrast, the *glmS* ribozyme has a $K_{1/2}$ for GlcN6P of at least 1 mM.

Cleavage by the *glmS* ribozyme results in the release of nucleotides 5′ of the scissile phosphate. In structures of the precleaved, sugar-bound *glmS* ribozyme complex, these nucleotides do not interact with GlcN6P; all of the nucleotides responsible for sugar binding are within the core of the RNA and are present in the product form of the ribozyme (*3, 9*). However, the initial structure of the cleaved form of the ribozyme from *T. tengcongensis* did not provide any evidence for GlcN6P bound in the active site (*9*). We independently solved the structure of the postcleavage form of the *glmS* ribozyme from *B. anthracis*. In one active site we see clear density for the entire molecule of GlcN6P, and in the other active sites we see density for at least the phosphate atom (Figure 3), suggesting that the *glmS* ribozyme retains affinity for GlcN6P following cleavage. The difference in cofactor binding between the *B. anthracis* structure reported here and the earlier *T. tengcongensis* structure is most likely a consequence of the *T. tengcongensis* crystals being grown at low pH (~5.3) where the $K_{1/2}$ for GlcN6P is ~6 mM (*10*). At this pH, the phosphate moiety of the sugar would be titrated to neutral, which would reduce the ability of the sugar to interact with Mg^{2+} and reduce the binding affinity. This is supported by the initial, low pH, *T. tengcongensis glmS* ribozyme structures where there is no evidence of metal ions coordinating the sugar phosphate.

Additionally, we solved the structure of an inactive mutant of the *B. anthracis glmS* ribozyme. In this ribozyme, the guanosine (G33) predicted to act as the general base to deprotonate the 2′-OH nucleophile has been mutated to an adenosine. A similar structure of the *T. tengcongensis* ribozyme has been reported by Klein et al. (*4*). This mutant ribozyme is extremely slow, over a factor of 10^5 less active than the wild-type *glmS* ribozyme (*3, 4*). In the mutant structure, the A is positioned in a similar way to the G in the wild-type structure (Figure 4). The only significant difference between the structure of the mutant and wild-type ribozymes is a slight shift in the position of the nucleotide leading to the loss of a hydrogen bond between the N1 of the purine and the 2′-OH nucleophile (*4*). This implicates G33 in the catalytic mechanism, acting not to position the 2′-OH, but in another role. Additionally, this nucleotide is located across the scissile phosphate from the GlcN6P binding pocket, and mutation of G33 appears to have no effect on GlcN6P binding, suggesting that G33 and the sugar cofactor play different roles in the catalytic mechanism.

Selectivity of the glmS Ribozyme against Noncognate Ligands. The *glmS* ribozyme is responsive to GlcN6P concentrations to regulate sugar levels within the cell. Activation of the ribozyme by ligands other than GlcN6P would deregulate this process and compromise the integrity of the bacteria. The feedback control mechanism of GlcN6P over the *glmS* gene would be circumvented by alternate sugars, both naturally occurring and foreign. Here we present two crystal structures of the *glmS* ribozyme bound to analogues of GlcN6P (Figure 5). One sugar, Glc6P, is structurally identical to GlcN6P with the substitution of oxygen (at C2) for nitrogen. The other sugar, MaN6P, is chemically identical to GlcN6P but has the stereochemistry inverted at C2. Both structures have RNA backbones that are superimposable with the structure of the *glmS* ribozyme bound to GlcN6P. These structures raise the question: How does the *glmS* ribozyme discriminate between GlcN6P and other similar sugars?

Glc6P is a naturally occurring, structurally similar, GlcN6P analogue. Most of the glucose that enters a cell is converted into Glc6P. There is clear density for the entire Glc6P molecule as well as the two coordinating magnesium ions, in all four active sites in the *B. anthracis glmS* crystal structure. However, the rate of the cleavage reaction with Glc6P is the same as the uncatalyzed rate (*18*). Further, there is some evidence that Glc6P can actually inhibit the reaction. Under subsaturating concentrations of GlcN6P, very high concentrations (10 mM) of Glc6P can reduce the rate of ribozyme cleavage (*18*). This indicates that although Glc6P is binding with at least moderate affinity to the *glmS* ribozyme, it is entirely unable to promote the reaction and suggests that the ribozyme discriminates against this sugar molecule using a catalytic mechanism.

How is the *glmS* ribozyme able to exclude molecules that contain a primary amine, which appears to be the key functional group for reactivity? All previous studies showed that deletion of that functional group on the small molecule led to cleavage rates for the *glmS* ribozyme similar to what is seen in the absence of small molecule activation (*5, 18*). Additionally, molecules that retain the primary amine and are able to activate the ribozyme, such as glucosamine and serinol, have much weaker apparent binding affinity than GlcN6P (*18*). These molecules are missing at least the phosphate moiety of the ligand. Presumably the deletion of functional groups is detrimental to binding as potential hydrogen-bonding partners are lost. Structures of the *B. anthracis glmS* ribozyme indicate that the phosphate moiety interacts with at least two Mg^{2+} ions, providing additional ionic interactions between the ligand and the ribozyme, an interaction that appears to be somewhat lost at low pH, where the phosphate becomes protonated and uncharged, thereby reducing its ability to coordinate Mg^{2+} and resulting in a significant increase of the $K_{1/2}$ of GlcN6P for the *glmS* ribozyme.

The *glmS* ribozyme is activated by the stereochemical analogue of GlcN6P, MaN6P. This molecule is chemically identical to GlcN6P, providing the same repertoire of functional groups as the natural ligand, but the stereochemistry is inverted at C2, which positions the primary amine on the same side of the sugar ring as the phosphate moiety. In the structure of the *glmS* ribozyme bound to MaN6P, there is only weak density observed for the sugar molecule in the active site of the ribozyme, but the molecule retains all of the same hydrogen-bonding partners as GlcN6P (Figure 5). We estimate the $K_{1/2}$ for MaN6P to be at least 20-fold higher than for GlcN6P. That such a slight change in the structure of the sugar molecule could impact the binding affinity of the ligand without having a similar effect on the rate suggests that there is a structural mechanism for discriminating against noncognate sugars (Figure 6).

Two mechanisms seem to be in play in the activation of the *glmS* ribozyme by small molecules. First, a chemical mechanism seems to be the driving force behind rejecting the GlcN6P mimic, Glc6P. Second, molecules with primary amines that retain the ability to activate the ribozyme appear to bind with significantly lower affinity than GlcN6P. This is even true for subtle changes, such as the inversion of the

stereochemistry of the C2-amine or lack of the phosphate group. By employing both of these mechanisms, the *glmS* ribozyme is able to select against ligands that are structurally and chemically similar to GlcN6P.

ACKNOWLEDGMENT

We thank H. Robinson, A. Heroux, S. Myers, A. Soares, and the beamline staff at X25 and X29 at the NSLS at Brookhaven National Laboratory; M. Strickler and the CSB core staff; A. Pyle and V. Serebrov for assistance with the quench-flow apparatus; and Y. Xiong, R. Breaker, P. Loria, J. Wang, D. Hiller, and members of the Strobel Laboratory for comments and discussions.

SUPPORTING INFORMATION AVAILABLE

Three figures and two tables as described in the text. This material is available free of charge via the Internet at http://pubs.acs.org.

REFERENCES

1. Cochrane, J. C., and Strobel, S. A. (2008) Catalytic strategies of self-cleaving ribozymes. *Acc. Chem. Res. 41*, 1027–1035.
2. Fedor, M. J., and Williamson, J. R. (2005) The catalytic diversity of RNAs. *Nat. Rev. Mol. Cell Biol. 6*, 399–412.
3. Cochrane, J. C., Lipchock, S. V., and Strobel, S. A. (2007) Structural investigation of the GlmS ribozyme bound to its catalytic cofactor. *Chem. Biol. 14*, 97–105.
4. Klein, D. J., Been, M. D., and Ferré-D'Amaré, A. R. (2007) Essential role of an active-site guanine in glmS ribozyme catalysis. *J. Am. Chem. Soc. 129*, 14858–14859.
5. Winkler, W. C., Nahvi, A., Roth, A., Collins, J. A., and Breaker, R. R. (2004) Control of gene expression by a natural metabolite-responsive ribozyme. *Nature 428*, 281–286.
6. Winkler, W. C., and Breaker, R. R. (2005) Regulation of bacterial gene expression by riboswitches. *Annu. Rev. Microbiol. 59*, 487–517.
7. Mandal, M., and Breaker, R. R. (2004) Gene regulation by riboswitches. *Nat. Rev. Mol. Cell Biol. 5*, 451–463.
8. Hampel, K. J., and Tinsley, M. M. (2006) Evidence for preorganization of the glmS ribozyme ligand binding pocket. *Biochemistry 45*, 7861–7871.
9. Klein, D. J., and Ferré-D'Amaré, A. R. (2006) Structural basis of glmS ribozyme activation by glucosamine-6-phosphate. *Science 313*, 1752–1756.
10. Klein, D. J., Wilkinson, S. R., Been, M. D., and Ferré-D'Amaré, A. R. (2007) Requirement of helix P2.2 and nucleotide G1 for positioning the cleavage site and cofactor of the glmS ribozyme. *J. Mol. Biol. 373*, 178–189.
11. Liu, M. Z., and Lee, Y. C. (2001) Comparison of chemical and enzymatic synthesis of 2-acetamido-2-deoxy-D-mannose 6-phosphate: a new approach. *Carbohydr. Res. 330*, 413–419.
12. McCoy, A. J., Grosse-Kunstleve, R. W., Storoni, L. C., and Read, R. J. (2005) Likelihood-enhanced fast translation functions. *Acta Crystallogr., Sect. D: Biol. Crystallogr. 61*, 458–464.
13. Otwinowski, Z., and Minor, W. (1997) Processing of X-ray diffraction data collected in oscillation mode. *Methods Enzymol. 276*, 307–326.
14. Emsley, P., and Cowtan, K. (2004) Coot: model-building tools for molecular graphics. *Acta Crystallogr., Sect. D: Biol. Crystallogr. 60*, 2126–2132.
15. Pannu, N. S., Murshudov, G. N., Dodson, E. J., and Read, R. J. (1998) Incorporation of prior phase information strengthens maximum-likelihood structure refinement. *Acta Crystallogr., Sect. D: Biol. Crystallogr. 54*, 1285–1294.
16. Winn, M. D., Isupov, M. N., and Murshudov, G. N. (2001) Use of TLS parameters to model anisotropic displacements in macromolecular refinement. *Acta Crystallogr., Sect. D: Biol. Crystallogr. 57*, 122–133.
17. DeLano, W. L. (2002) The PyMOL Molecular Graphics System, DeLano Scientific, San Carlos, CA.
18. McCarthy, T. J., Plog, M. A., Floy, S. A., Jansen, J. A., Strauss-Soukup, J. K., and Soukup, G. A. (2005) Ligand requirements for glmS ribozyme self-cleavage. *Chem. Biol. 12*, 1221–1226.
19. Lim, J., Grove, B. C., Roth, A., and Breaker, R. R. (2006) Characteristics of ligand recognition by a glmS self-cleaving ribozyme. *Angew. Chem., Int. Ed. Engl. 45*, 6689–6693.
20. Mandal, M., Boese, B., Barrick, J. E., Winkler, W. C., and Breaker, R. R. (2003) Riboswitches control fundamental biochemical pathways in *Bacillus subtilis* and other bacteria. *Cell 113*, 577–586.
21. Mandal, M., Lee, M., Barrick, J. E., Weinberg, Z., Emilsson, G. M., Ruzzo, W. L., and Breaker, R. R. (2004) A glycine-dependent riboswitch that uses cooperative binding to control gene expression. *Science 306*, 275–279.
22. Stryer, L. (1995) *Biochemistry*, 4th ed., W. H. Freeman, New York.

BI802069P